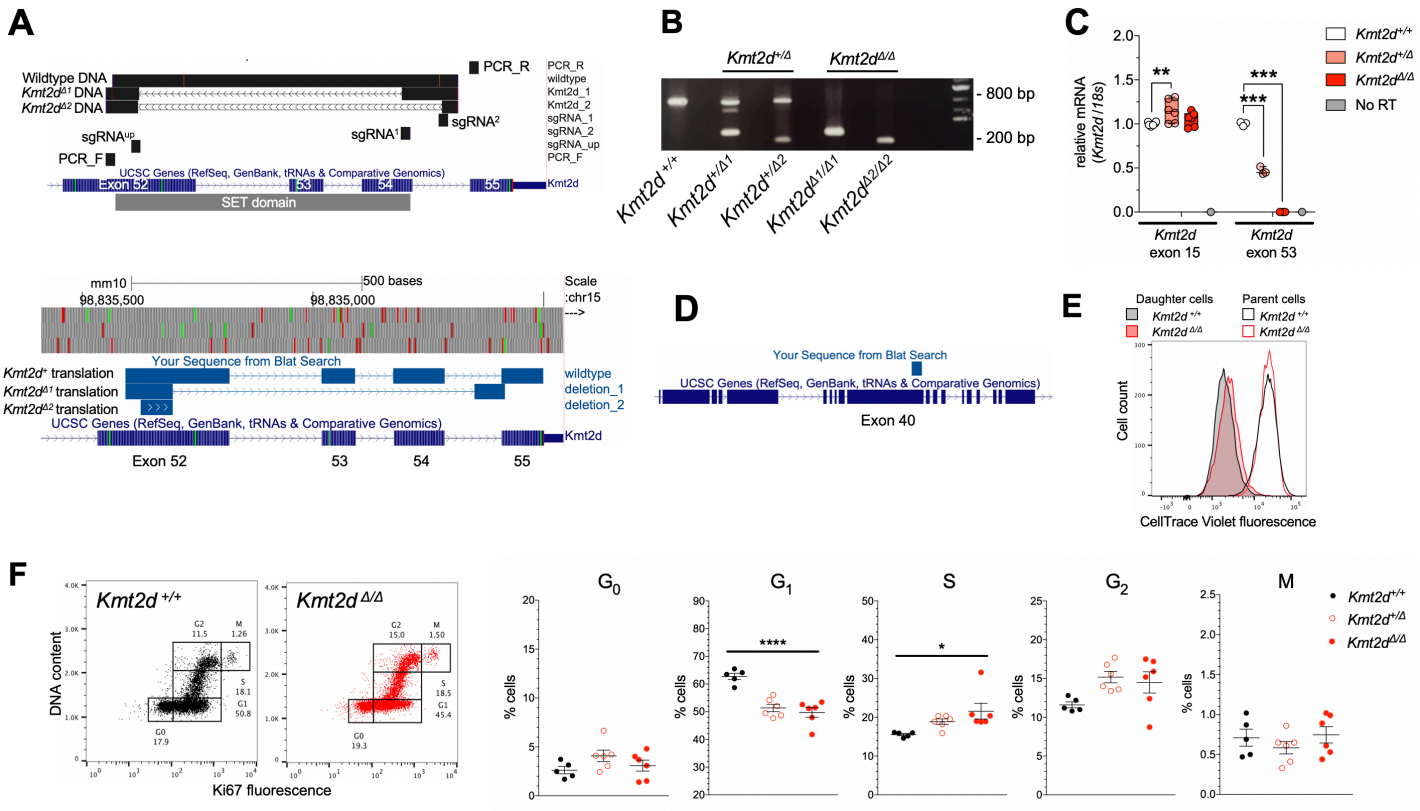

Supplementary Figure 1. CRISPR-targeted HT22 cells. (**A**) Sanger-sequenced DNA of wild-type (*Kmt2d*$^{+}$) and targeted (*Kmt2d*$^{\Delta}$) alleles in HT22 cells, mapped with sgRNAs and PCR primers, to *Kmt2d* locus (mm10) on chromosome 15. Mapping of Sanger-sequenced DNA after in silico translation to predict amino acid sequences illustrates premature termination codons (PTC) created in *Kmt2d*$^{\Delta 1}$ and *Kmt2d*$^{\Delta 2}$ alleles. (**B**) PCR with probes flanking sgRNA cut sites identifies experimental cell lines (*Kmt2d* $^{+/\Delta}$ and *Kmt2d*$^{\Delta/\Delta}$) compared to wild-type (*Kmt2d*$^{+/+}$). (**C**) RT-qPCR analysis of mRNA using probes spanning upstream exons (15-16) or exons within the deletion site (53-54). Two-way ANOVA with post hoc multiple comparisons. (**D**) Mapped peptide sequence of KMT2D antibody (Sigma). (**E**) Flow cytometric CellTrace fluorescence after 72 hours in HT22 cells. Increased intensity indicates less dye dilution, i.e. fewer cell divisions in mutants (left). Parental cell data confirm genotype-independent dye uptake (right) at 0 hours. (**F**) Cell cycle gating by flow cytometric analysis using Ki67 and DAPI to discriminate individual stages (G_0, G_1, S, G_2, M) in *Kmt2d*$^{+/+}$ and *Kmt2d*$^{\Delta/\Delta}$ cells, and quantification of each cycle phase. One-way ANOVA. Bars indicate mean ± SEM. Boxes indicate mean ± interquartile range; whiskers indicate minima and maxima. (*p<0.05, **p<0.01, ***p<0.001, ****p<0.0001).

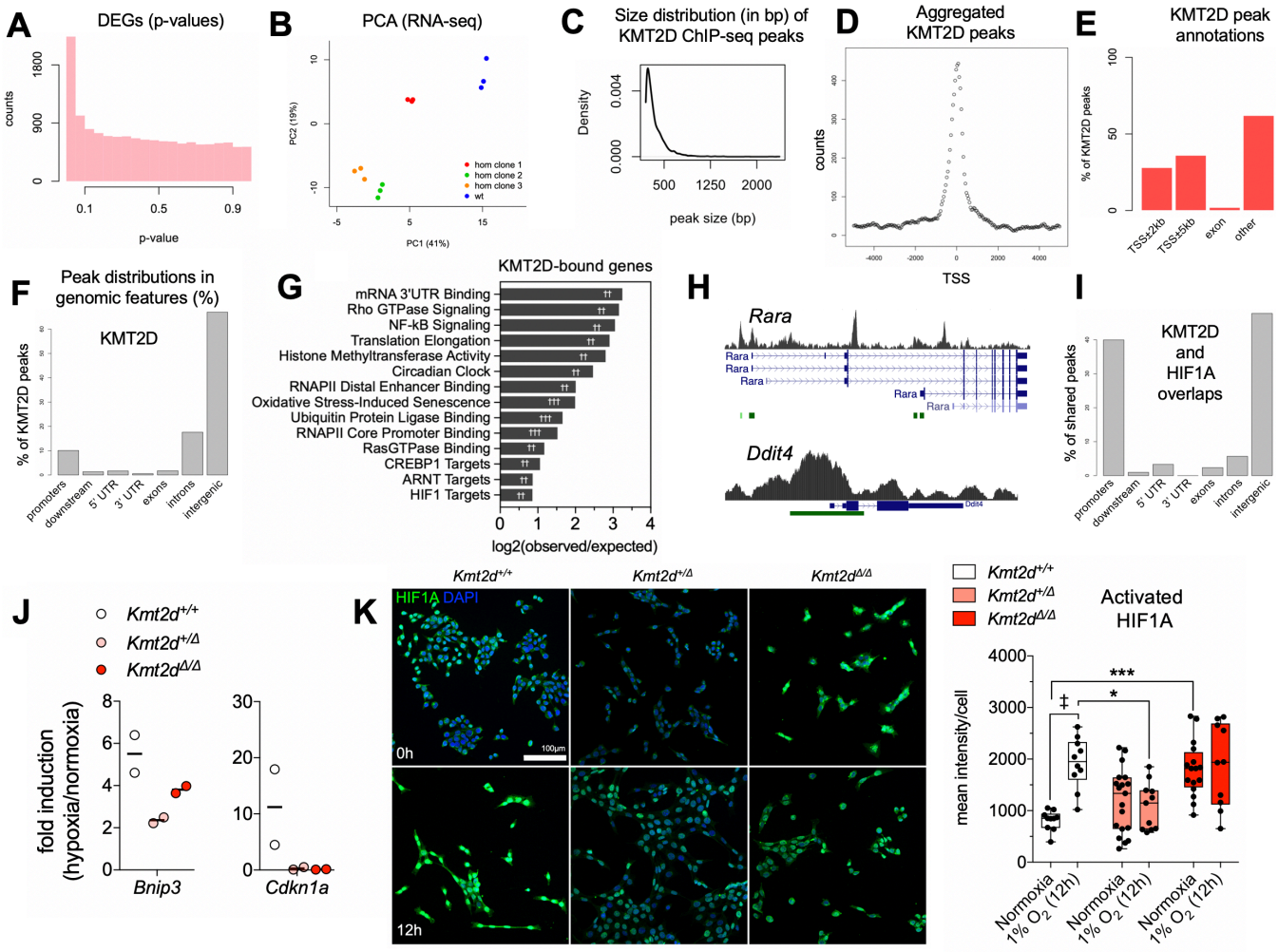

Supplementary Figure 2. HT22 cell RNA-seq and ChIP-seq analysis. (**A**) P-value distribution in *Kmt2d*$^{\Delta/\Delta}$ DEGs relative to wild-type indicates a well-calibrated test. (**B**) PCA visualizing clear expression differences in wild-type and *Kmt2d*$^{\Delta/\Delta}$ HT22 cells. (**C**) The size distribution (in bp) of KMT2D ChIP-seq peaks. (**D**) Validation of KMT2D peak distributions about gene TSSs and (**E-F**) genomic features. (**G**) Gene networks showing highest fold change in enrichment among genes proximal to KMT2D peaks (TSS±5 kb). Fisher's Exact Test (†FDR<0.05, ††FDR<0.01, †††FDR<0.001). (**H**) KMT2D peaks clustered at alternate TSSs of *Rara* gene and enhancer-like peaks at *Ddit4* gene. (**I**) Genomic features at overlapping KMT2D and HIF1A (26) ChIP-seq peaks. (**J**) RT-qPCR analysis of hypoxia-induced gene expression in HT22 cells, upon 1% O_2 exposure. One-way ANOVA (n.s.). (**K**) HIF1A nuclear fluorescence, i.e. activation, analysis. Representative z-stacked confocal images are shown with quantifications of nuclear HIF1A fluorescence. Two-way ANOVA with post hoc multiple comparisons (significance from wild-type, *p<0.05, **p<0.01, ***p<0.001; and from baseline, ‡p<0.01). Boxes indicate mean ± interquartile range; whiskers indicate minima and maxima. Scale bar 100 μm.

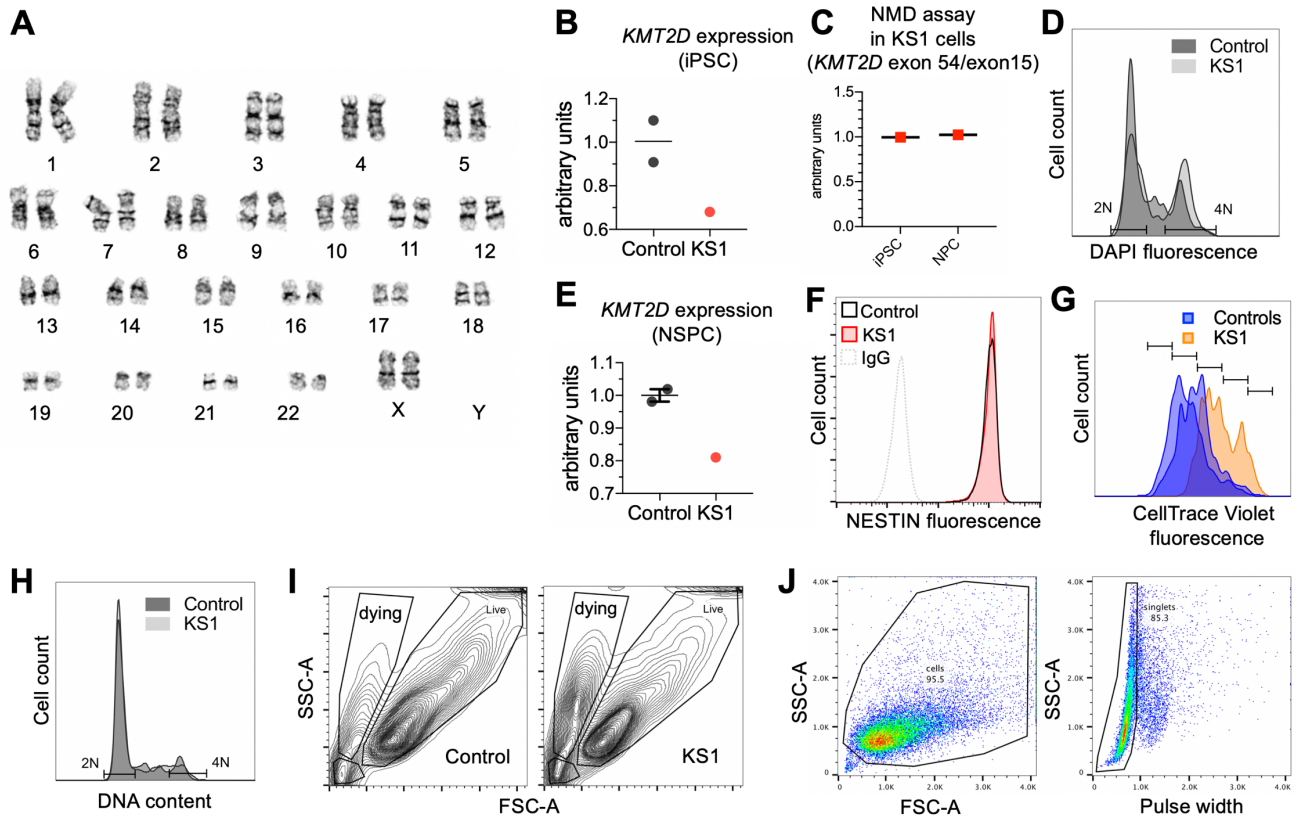

Supplementary Figure 3. iPSC and NSPC line validations and additional phenotyping. (**A**) 46, XX normal female karyotype in KS1-1 iPSCs. (**B**) RT-qPCR analysis of *KMT2D* (exon 15) expression in KS1 iPSCs compared to two healthy control iPSC lines (C1-2 and C3-1). Dots represent average of technical triplicates per patient line. Bars indicate mean. (**C**) RT-qPCR demonstrating equivalent exonic ratios of *KMT2D* exon 15 to exon 54, measured in technical triplicate, consistent with NMD of the entire transcript. (**D**) Flow cytometric analysis of DNA content by DAPI fluorescence in iPSCs. (**E**) RT-qPCR analysis of *KMT2D* (exon 15) expression in NSPCs derived from the KS1 and control iPSC lines, measured in technical triplicate. (**F**) Flow cytometric analysis of NES fluorescence intensity in KS1 and control NSPCs. (**G**) CellTrace Violet generational tracking showing fewer divisions (i.e. higher dye intensity) in patient-derived NSPCs over 72 hours. (**H**) Flow cytometric analysis of DNA content by DAPI fluorescence in NSPCs. (**I**) Sample flow cytometric gating for detection of scatter profiles indicative of cell death-associated cellular condensation. (**J**) Representative gating of viable cells and doublet discrimination in immunofluorescence-based flow cytometric analyses of iPSCs and NSPCs.

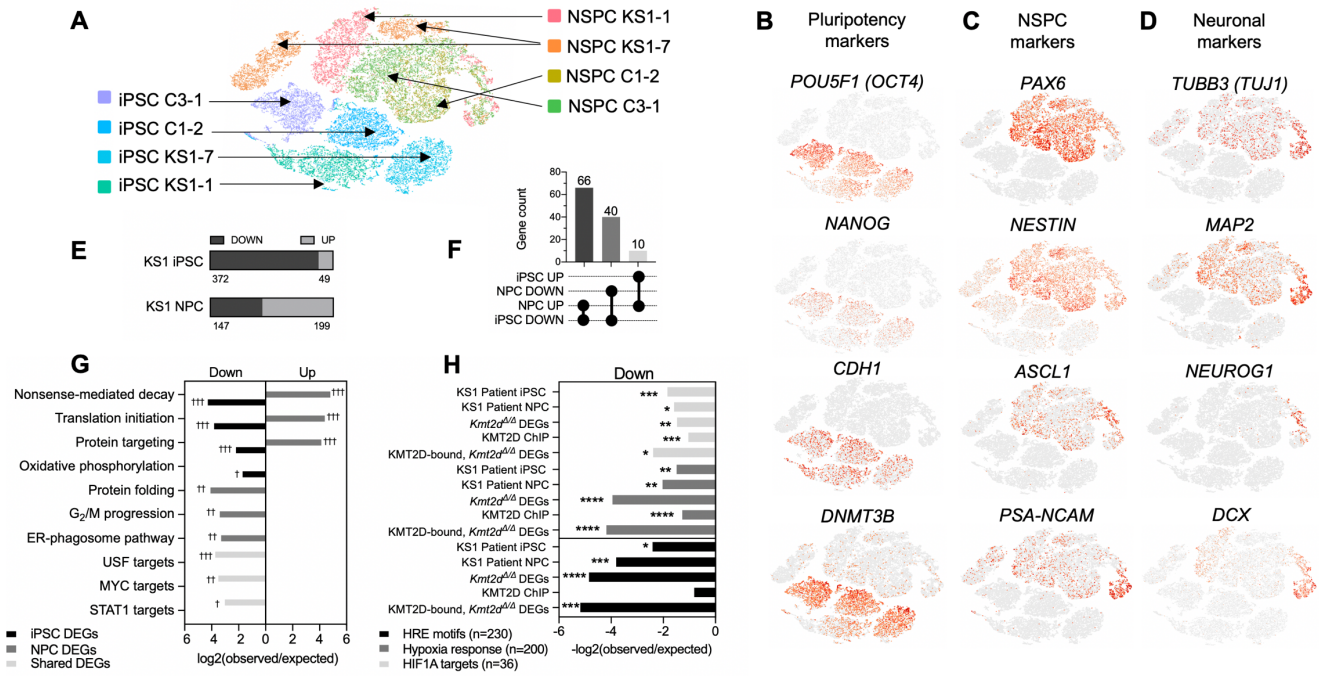

Supplementary Figure 4. iPSC and NSPC single-cell RNA-seq analysis. (**A**) t-stochastic neighbor embedding (tSNE) representation of iPSC and NSPC libraries sequenced on 10XGenomics platform. Cell clusters colored by cell type and patient ID. iPSCs and NSPCs derived from patient K1-7 were excluded from downstream analysis due to abnormal karyotype. (**B-D**) Representative tSNE of iPSC, NSPC, and neuronal markers demonstrating expected cell identities and revealing a gradient of cell maturation. (**E**) Proportions of DEGs down- or up-regulated in KS1 patient iPSCs or NSPCs compared to respective healthy controls, (**F**) DEG lists intersected for overlaps among down-regulated and up-regulated genes, and (**G**) Gene networks most enriched among differentially expressed genes (DEGs) in KS1 patient iPSCs and NSPCs relative to respective healthy controls, and DEGs shared in both cell types. (**H**) Significant enrichments of Hypoxia Response genes, HIF1A Direct Target genes, and genes containing the Hypoxia Response Element (HRE) RCGTG motif among observed DEGs in KS1 Patient iPSCs, KS1 Patient NSPCs, *Kmt2d*$^{\Delta/\Delta}$ HT22 cells, as well as KMT2D-bound genes in wild-type HT22 cells, and KMT2D-bound, down-regulated genes in *Kmt2d*$^{\Delta/\Delta}$ HT22 cells). Fisher's Exact Test (*p<0.05, **p<0.01, ***p<0.001; †FDR<0.05, ††FDR<0.01, †††FDR<0.001).

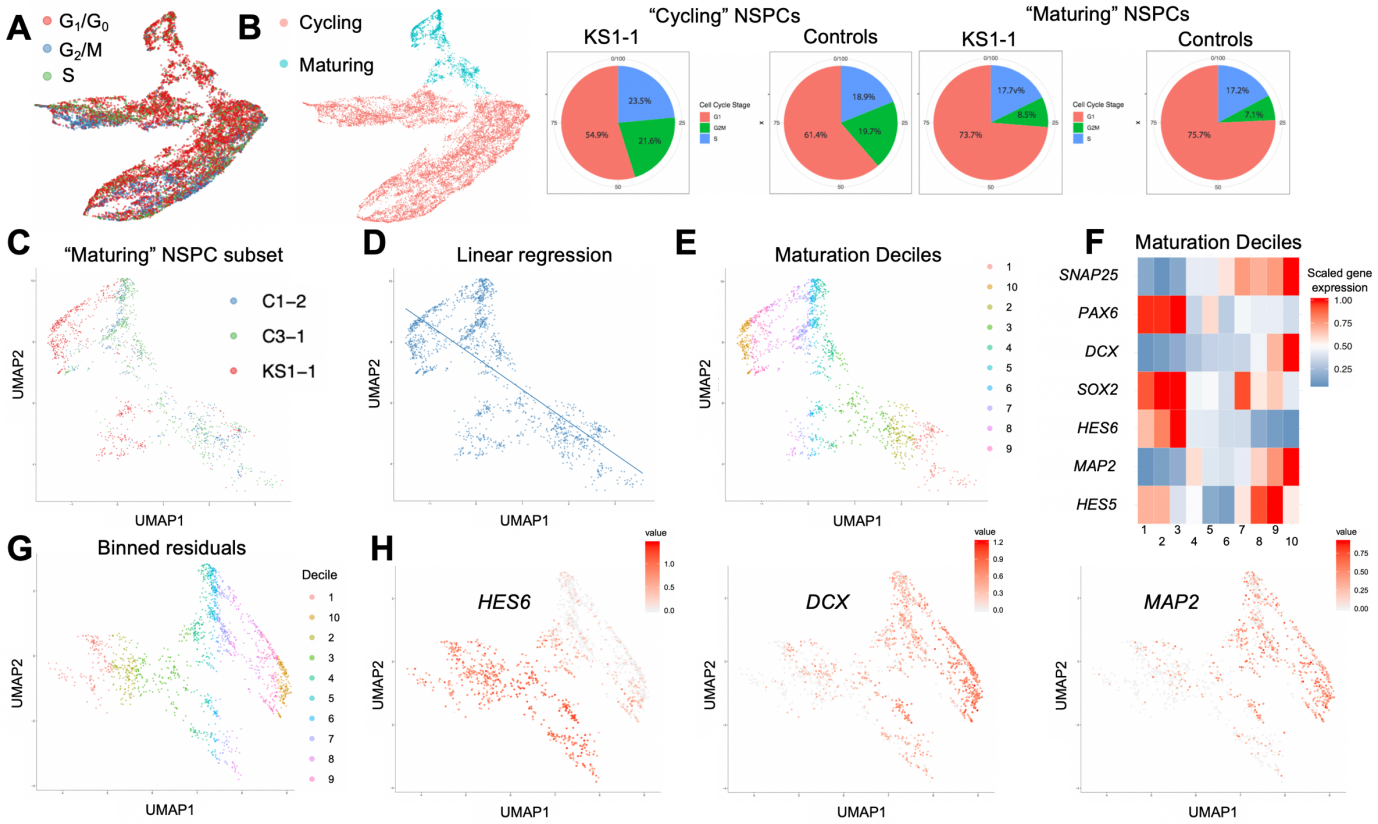

Supplementary Figure 5. Stratified scRNA-seq analysis of NSPCs. Uniform Manifold Approximation Projection (UMAP) of single-cell NSPC libraries partitioned by (**A**) cell cycle marker expression into subsets of G_1/G_0, S, and G_2/M cells, used for cycle phase-stratified differential expression analysis to rule out confounding differences in cell cycle phase composition on NSPC transcriptome comparisons. (**B**) Subset of "Cycling" versus non-cycling, "Maturing" NSPCs, which includes "Transitioning" and "Differentiating" cells as defined (**Figure 4B**), and UMAP-based cell cycle occupancies consistent with experimental FACS data (**Figure 3F**). (**C-H**) UMAP analysis of Differentiating NSPCs displaying (**C**) library patient ID's, (**D**) smooth linear regression fitted to define the maturation trajectory and (**E**) binned deciles of progressively maturing cells along the regression. (**F**) Relative expression of selected NSPC markers defining directionality of the maturation trajectory. (**G**) Binned residuals used to calculate deciles containing equal number of cells along the axis of differentiation. (**H**) Representative NSPC marker expression plotted over binned residuals.

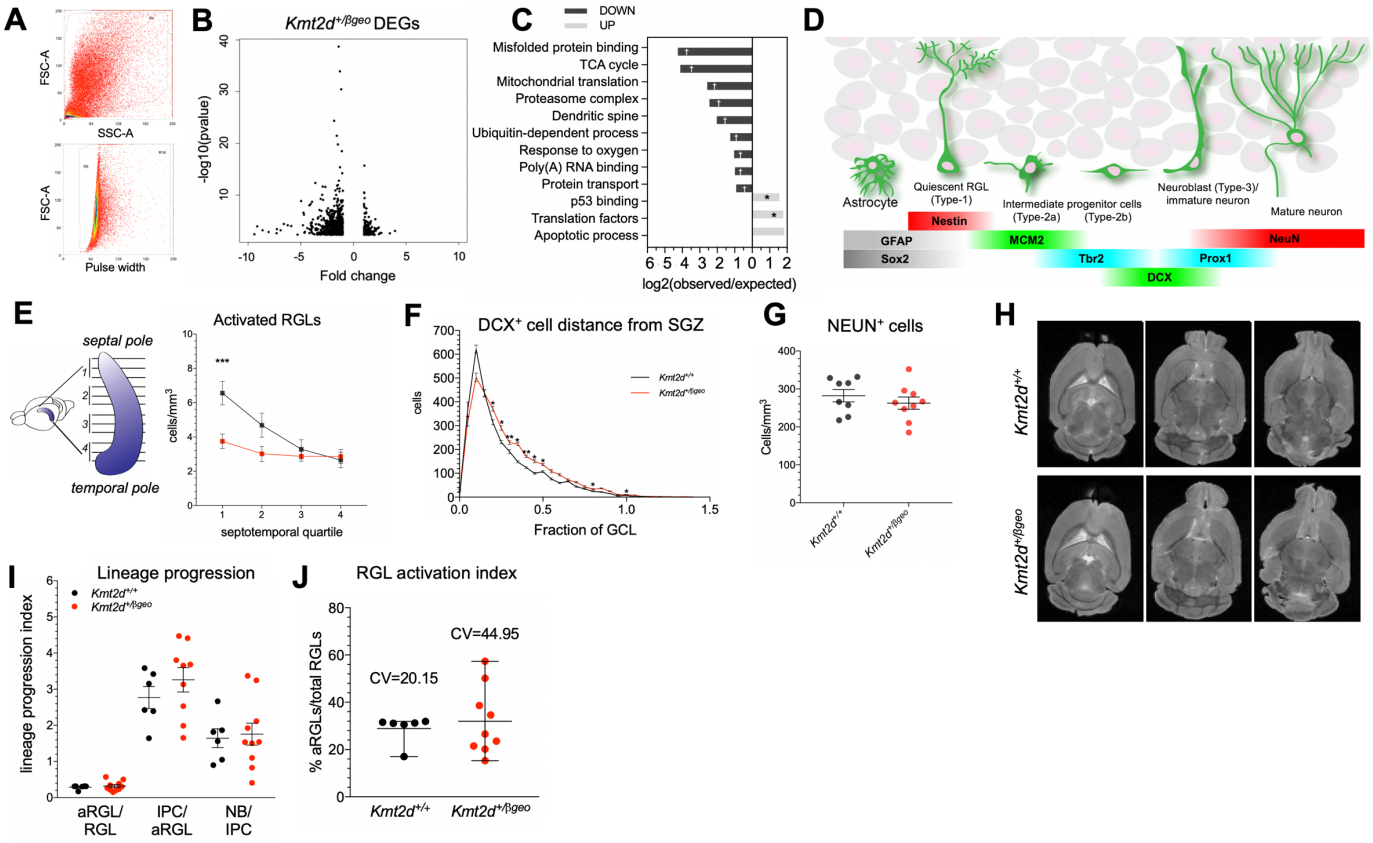

Supplementary Figure 6. Phenotyping of *Kmt2d*$^{+/\beta geo}$ mice. (**A**) Sample FACS gating for viable nuclei and doublet discrimination during purification of cycling EdU^{+} nuclei purified from *Kmt2d*$^{+/+}$ and *Kmt2d*$^{+/\beta geo}$ mice at 16 hours post-EdU pulse for RNA-seq and cell cycle analysis. (**B**) RNA-seq analysis of differential gene expression in purified EdU^{+} DG nuclei from *Kmt2d*$^{+/+}$ and *Kmt2d*$^{+/\beta geo}$ mice. (**C**) Gene networks most enriched among DEGs down- or up-regulated in *Kmt2d*$^{+/\beta geo}$ nuclei, showing transcriptional suppression of cellular metabolic pathways. Fisher's Exact Test (†FDR<0.05, ††FDR<0.01, †††FDR<0.001). (**D**) Schematic depicting marker expression during sequential stages of adult DG neurogenesis. (**E**) Serial ordering of perfusion-fixed brain slices enables anatomically-stratified analysis of neurogenesis, for quantification of activated RGL NSPC density along the septotemporal axis of the DG in *Kmt2d*$^{+/+}$ and *Kmt2d*$^{+/\beta geo}$ mice, indicating preferential disruption at the septal DG. Two-way ANOVA with post hoc multiple comparisons. (**F**) Quantification of DCX^{+} NB cell body distance from SGZ plane in 8-week-old mice (9-10 mice per genotype, >1,000 cells per mouse). Two-way ANOVA with post hoc multiple comparisons. (**G**) Quantification of RBFOX3/NEUN^{+} mature DG neurons in 8-week-old mice (8-9 mice per genotype, 10 z-stacks per mouse). Student's t-test (n.s.). (**H**) Sample images of T2-weighted MRI (9.4T) in PFA-fixed brains of female mice 4 months old. (**I**) Comparison of lineage progression index, an approximation of expansion potential for each cell type transition, indicates absence of genotype-associated blockages at any particular cell-type transition analyzed, and (**J**) increased Coefficient of Variance (CV) in RGL activation rates in *Kmt2d*$^{+/\beta geo}$ mice. Bars indicate mean ± SEM. (*p<0.05, **p<0.01, ***p<0.001).

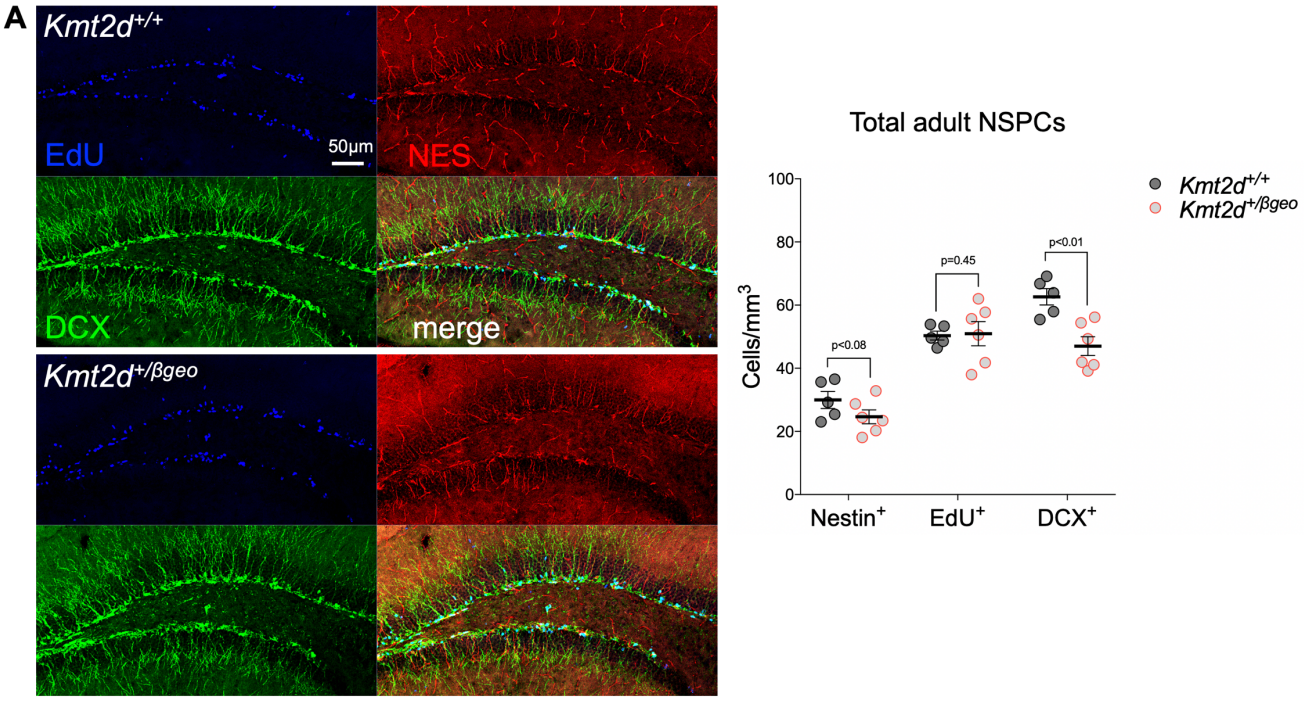

Supplementary Figure 7. Pulse-labeling to birth-date adult-born NSPCs in vivo. (**A**) Representative immunostaining from *Kmt2d*$^{+/+}$ and *Kmt2d*$^{+/\beta geo}$ mice (5-6 mice per genotype, 10 z-stacks per mouse) of EdU pulse-labeled cells extending a NES^{+} process (early RGL NSPCs) or DCX^{+} process (maturing NB NSPCs), showing the entire DG area quantified. Steady-state quantification of NSPCs and EdU-labeled NSPCs, confirming steady-state reduction of adult neurogenesis in *Kmt2d*$^{+/\beta geo}$ mice, despite their increased number of EdU^{+}DCX^{+} double-labeled NBs in the same experiment (**Figure 5E-F**). Bars indicate mean ± SEM, Student's t-test. Scale bar 50 μm.

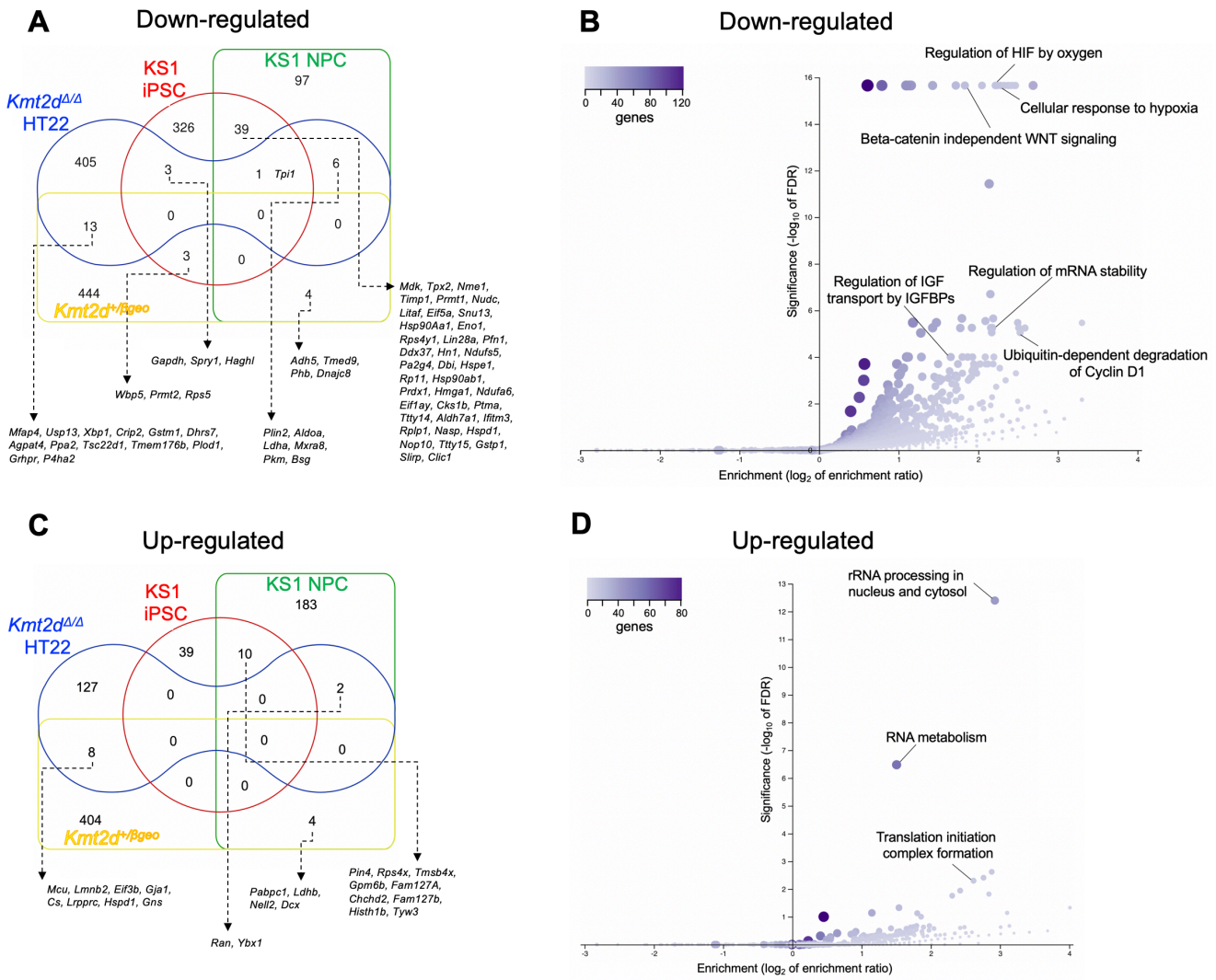

Supplementary Figure 8. Comparison of gene expression across KS1 models. (**A-B**) Euler diagram depicting shared transcriptional downregulation in KS1 models with individual genes (**A**) and pathways enriched among down-regulated genes from all KS1 models presently studied (**B**). (**C-D**) Euler diagram depicting transcriptional upregulation in KS1 models with individual genes (**C**) and pathways enriched among up-regulated genes from all KS1 models presently studied (**D**). Enrichments expressed as $\log_2$ of enrichment ratio. Significance expressed as $-\log_{10}$ of FDR. (WebGestalt).

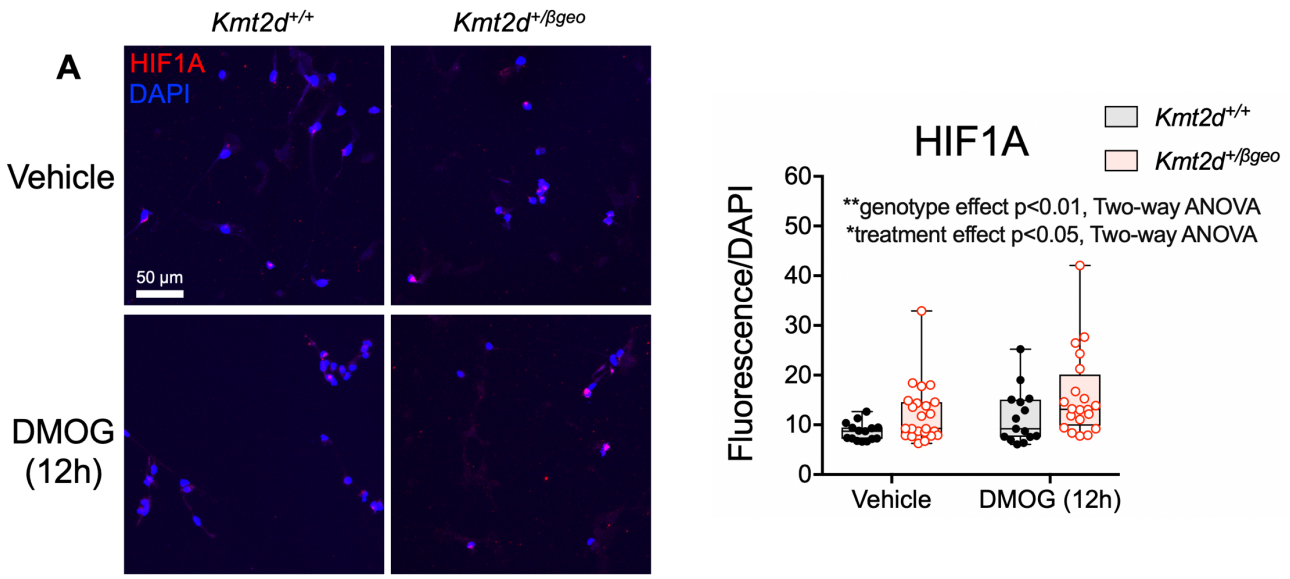

Supplementary Figure 9. HIF1A activation in primary hippocampal NSPCs. (**A**) Representative confocal images of primary hippocampal NSPCs isolated from micro-dissected DG of *Kmt2d*$^{+/+}$ and *Kmt2d*$^{+/\beta geo}$ mice, with quantification for analysis of HIF1A fluorescence inside the nucleus (DAPI^{+} volume). Two-way ANOVA with post-hoc multiple comparisons. (*p<0.05, **p<0.01, ***p<0.001). Boxes indicate mean ± interquartile range; whiskers indicate minima and maxima. Scale bar 50 µm.

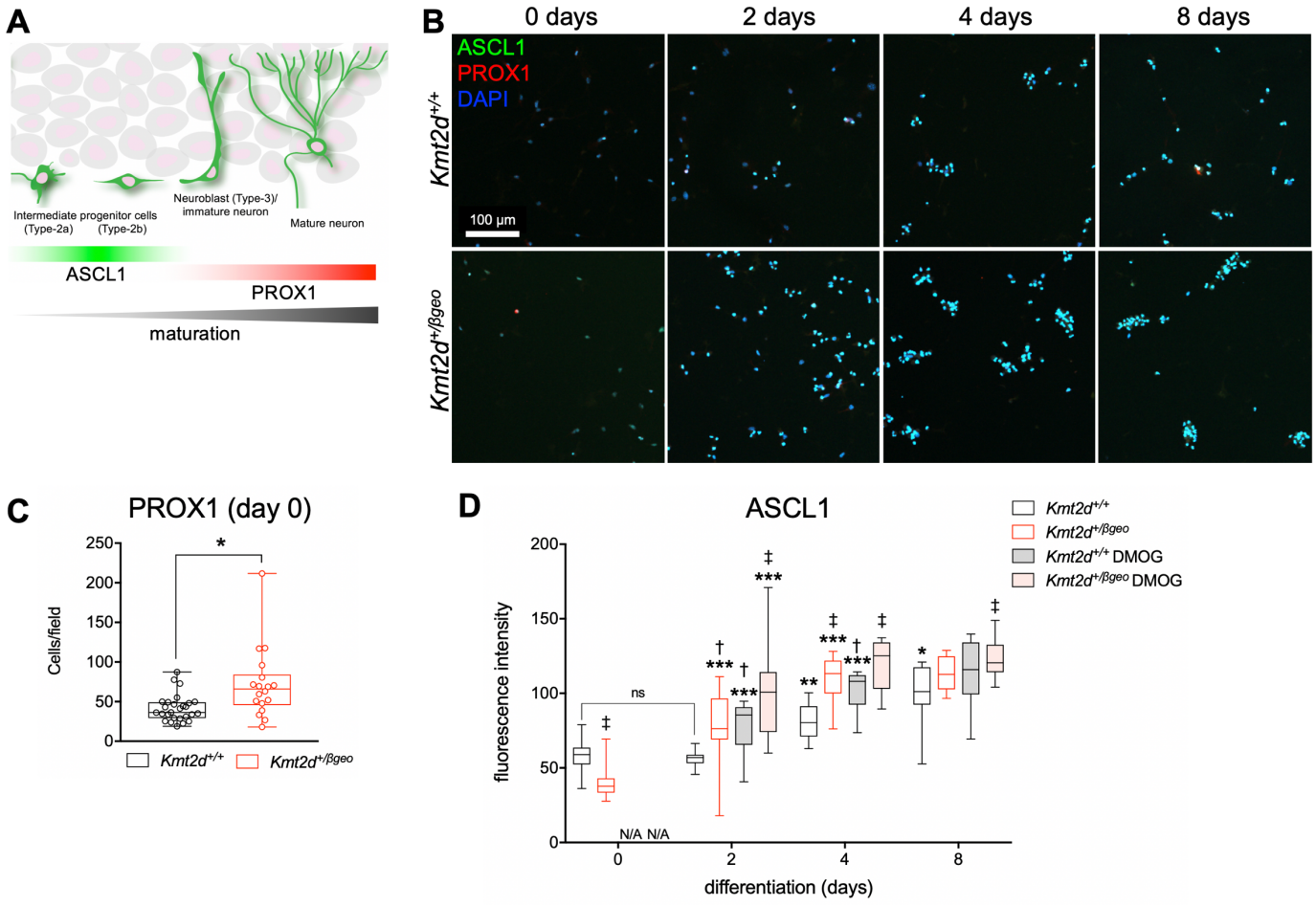

Supplementary Figure 10. Precocious in vitro differentiation of primary hippocampal NSPCs. (**A**) Schematic depicting developmental expression of pro-neural transcription factor ASCL1 and maturing neuronal marker PROX1 in adult-born DG neurons. (**B**) Representative confocal images for analysis of NSPCs differentiating between 0 and 8 days in primary hippocampal NSPCs isolated from micro-dissected DG of *Kmt2d*$^{+/+}$ and *Kmt2d*$^{+/βgeo}$ mice, with quantifications (**C-D**). 22,307 cells analyzed individually across 176 fields of view. Two-way ANOVA with post hoc multiple comparisons. Boxes indicate mean ± interquartile range; whiskers indicate minima and maxima. (significance from previous time point *p<0.05, **p<0.01; ***p<0.001; significance from vehicle-treated wild-type †p<0.05, ‡p<0.01). Scale bar 100 µm.